PERGAMON

International Journal of Solids and Structures 38 (2001) 9033–9051

INTERNATIONAL JOURNAL OF SOLIDS and STRUCTURES

www.elsevier.com/locate/ijsolstr

Effects of piezoelectric sensor/actuator debonding on vibration control of smart beams

Dongchang Sun [a], Liyong Tong [a,*], Satya N. Atluri [b]

[a] *School of Aerospace, Mechanical and Mechatronic Engineering, Building J07, The University of Sydney, Sydney, NSW 2006, Australia*
[b] *Department of Mechanical and Aerospace Engineering, University of California, Los Angeles, CA 90095-1600, USA*

Received 16 December 2000; in revised form 24 July 2001

Abstract

In vibration control of smart structures, piezoelectric sensors/actuators are usually bonded to the surface of a host structure. Debonding may occur between the piezoelectric sensors/actuators and the host structure, and it may decrease the control efficiency of vibration suppression or even lead to an unstable closed loop control system. This paper investigates the effect of the debonding on vibration control of beams with piezoelectric sensors and actuators. Presented is a novel model, which takes into account both flexural and longitudinal displacements of the host beam and piezoelectric layers as well as the peel and shear strains of the adhesive layer. Both collocated and non-collocated control schemes are used to study the effects of sensor or actuator debonding on active vibration control of smart beams.

Keywords: Modeling; Vibration damping; Debonding; Piezoelectric transducers; Smart structures

1. Introduction

Vibration control of flexible structures by distributed piezoelectric sensors and actuators has been widely studied in the past decade and more dimensions are introduced to improve control of structural behavior (See e.g. Baz and Poh, 1988; Im and Atluri, 1989; Shi and Atluri, 1990; Lee and Moon, 1990; Tzou and Anderson, 1992; Chandrashekhara and Agarwal, 1993; Gu et al., 1994; Crawley, 1994; Sun et al., 1999; Chee et al., 1998; Sun and Tong, 2001a,b). As one of the most widely used smart materials, piezoelectric materials are usually surface bonded on or embedded into the host structures as distributed sensors and actuators. In most of the previous studies, it is assumed that piezoelectric actuators and sensors are perfectly bonded to the host structures. However, debonding between the piezoelectric layers and the host structures may occur during its service life. For example, high peel stresses may be created around the periphery of an actuator layer. This is particularly true when single crystal layers are used as actuators due to its extremely high breakdown voltage. When a full range of an electric filed is applied to a single crystal

* Corresponding author. Tel.: +61-2-9351-6949; fax: +61-2-9351-4841.
E-mail address: ltong@aeromech.usyd.edu.au (L. Tong).

0020-7683/01/$ - see front matter
PII: S0020-7683(01)00180-9

layer, high peel stresses may be developed even for a very thin layer. As a result of debonding, dynamic characteristics of an open loop system, the sensing and actuating behaviors of a sensor and actuator may be changed, and the properties of a closed loop system may be affected severely or even destabilized. Therefore investigating the effects of partial debonding of the piezoelectric actuator/sensor patches on active control of smart structures is of significant importance in addressing damage tolerance issues of smart structures.

A significant amount of studies have been conducted on modeling of delamination of composite structures. Delamination detection of the composite structures by using perfectly bonded/embedded piezoelectric sensor layer and actuator layer structures has also attracted increasingly attention in recent years. However, there exists a relatively less literature on modeling and control of flexible structures with partially debonded piezoelectric sensors and actuators. Seeley and Chattopadhyay (1999) developed a finite element model for the structures including actuator debonding based on a refined high order theory (HOT). In this model, the displacement continuity in the interface between the debonded and non-debonded areas is imposed and implemented using a penalty approach. They also conducted experimental investigation on vibration control of a composite beam with debonded piezoelectric actuator (Seeley and Chattopadhyay, 1998), and found that the debonding length is a critical factor to the closed-loop control. For the static case, Wang and Meguid (2000) analytically examined the static effect of the partial debonding of the actuator from the host structures under plane strain assumption.

To better understand the effect of debonding of the piezoelectric sensor/actuator on closed-loop vibration control of a beam, an analytical model of the beam with piezoelectric sensor and actuator layer including debonding is presented in this paper. In this model, both longitudinal and transverse vibrations are considered using classical beam theory. Taking the displacements and their corresponding internal forces as the state variables, a numerical approach based on the multiple shooting method is employed to solve the equations, and the continuity of displacements and the internal forces at the interfaces between the debonded and non-debonded areas can be ensured. Using this model, examined are the debonding effects on closed-loop vibration control of smart beams using two kinds of control laws.

2. Modeling of beam with debonded actuator/sensor

2.1. Governing equations

Consider a slender beam, on which several piezoelectric patch pairs are bonded, as shown in Fig. 1. The debonding between the piezoelectric patches and the host beam is assumed to occur throughout the width of the beam. It is also assumed that the shear and peeling strains in the adhesive layer are constants along its

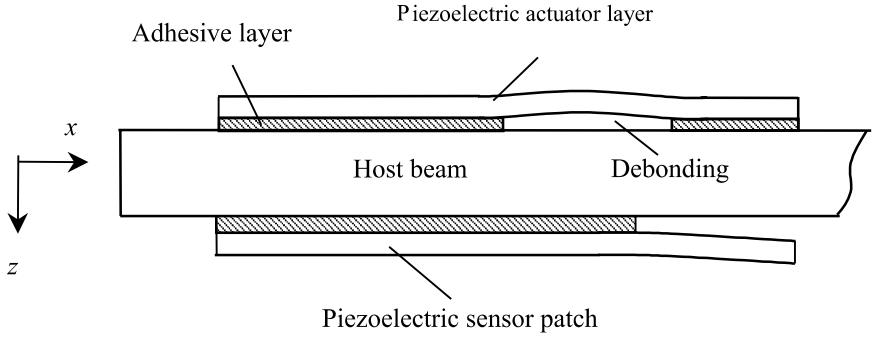

Fig. 1. The beam and piezoelectric layer with debonding.

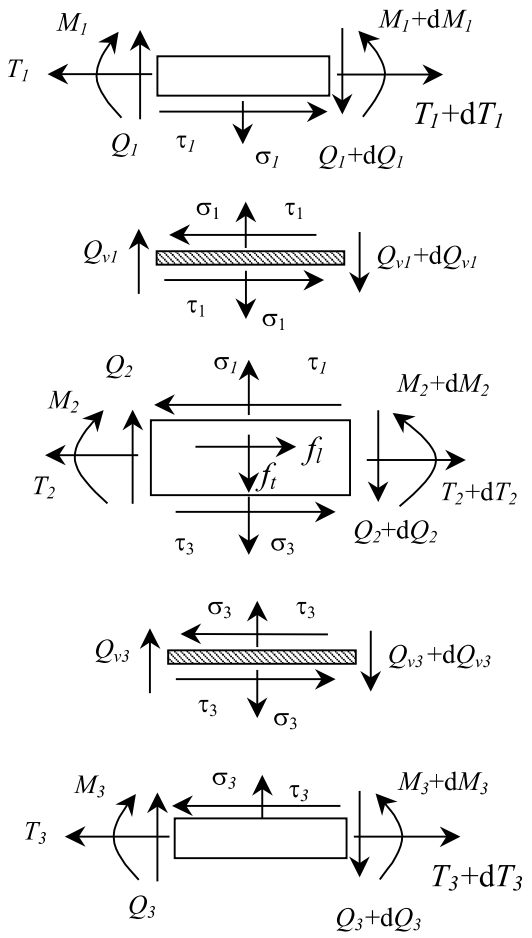

Fig. 2. Free-body diagram of the beam with piezoelectric patches.

thickness, and that there is no stress transfer between the host beam and the piezoelectric patch in the debonding portion.

The entire composite beam can be divided into several segments, the segments containing only the host beam, and the segments including the host beam bonded with two piezoelectric patches on its upper and lower surfaces. The piezoelectric patch pair may function as either sensor pair or actuator pair or even collocated actuator/sensor couple depending on the selected control scheme. For the segment including host beam and piezoelectric patches, its free-body diagram is shown in Fig. 2, and from this figure the following equations of motion can be obtained

$$\rho_1 u_{1,tt} = T_{1,x} + b\tau_1 \tag{1a}$$

$$\rho_1 w_{1,tt} = Q_{1,x} + b\sigma_1 \tag{1b}$$

$$M_{1,x} + b\tau_1 h_1/2 - Q_1 = 0 \tag{1c}$$

$$\rho_2 u_{2,tt} = T_{2,x} - b\tau_1 + b\tau_3 + f_l(x,t) \tag{2a}$$

$$\rho_2 w_{2,tt} = Q_{2,x} - b\sigma_1 + b\sigma_3 + f_t(x,t) \tag{2b}$$

$$M_{2,x} + b(\tau_1 + \tau_3)h_2/2 - Q_2 = 0 \tag{2c}$$

$$\rho_3 u_{3,tt} = T_{3,x} - b\tau_3 \tag{3a}$$

$$\rho_3 w_{3,tt} = Q_{3,x} - b\sigma_3 \tag{3b}$$

$$M_{3,x} + b\tau_3 h_3/2 - Q_3 = 0 \tag{3c}$$

where the subscripts 1, 2 and 3 represent the upper piezoelectric layer, the host beam and the lower piezoelectric layer, respectively, the subscripts ,t and ,x denote the partial differentiation with respect to t and x respectively, u is the longitudinal displacement in mid-plane, w is the transverse displacement, h denotes the thickness, b is the width of the composite beam, τ and σ are the shear and peel stress of the adhesive layer, T, Q and M are the axial force, transverse shear force and bending moment respectively, and $f_l(x,t)$ and $f_t(x,t)$ are the axial and transverse loads per unit length, and ρ_i $(i = 1,2,3)$ are the equivalent mass densities per unit length of the three layers in which the mass of the adhesive layers is considered.

Based on the constitutive equation of the piezoelectric materials, the following equations can be obtained

$$\begin{aligned} T_i &= \bar{A}_i u_{i,x} - \bar{B}_i w_{i,xx} - b e_{31i} V_i \\ M_i &= \bar{B}_i u_{i,x} - \bar{D}_i w_{i,xx} - b e_{31i} r_i V_i \end{aligned} \quad i = 1,2,3 \tag{4}$$

where e_{31i} is the piezoelectric stress constant (for the host beam, $e_{312} = 0$), r_i the z-coordinate value of the mid-plane of the three layer from their own neutral plane, V_i the voltage applied on the three layers along their thickness direction, $\overline{A}_i$ and $\overline{D}_i$ the axial and bending stiffness, and $\overline{B}_i$ the extension-bending coupling term.

The shear and peel stress in the adhesive layer with debonding can be modeled as follows:

$$\tau_1 = k_1 G_{v1}\left[\frac{1}{2h_{v1}}(h_1 w_{1,x} + h_2 w_{2,x}) + \frac{u_2 - u_1}{h_{v1}}\right] \tag{5a}$$

$$\tau_3 = k_3 G_{v3}\left[\frac{1}{2h_{v3}}(h_2 w_{2,x} + h_3 w_{3,x}) + \frac{u_3 - u_2}{h_{v3}}\right] \tag{5b}$$

$$\sigma_1 = k_1(1-v)Y_{v1}/((1-2v)(1+v)h_{v1})(w_2 - w_1) \tag{6a}$$

$$\sigma_3 = k_3(1-v)Y_{v3}/((1-2v)(1+v)h_{v3})(w_3 - w_2) \tag{6b}$$

where h_v is the thickness of the adhesive layer, Y_v and G_v are the Young's modulus and shear modulus respectively, v is the Poisson's ratio of the adhesive layers, k_1 and k_3 are parameters characterizing the bonding conditions between the piezoelectric layers and the host beam,

$$k_i = \begin{cases} 0 & \text{debonding} \\ 1 & \text{perfect bonding} \end{cases} \quad i = 1,3 \tag{7}$$

In the debonding area between the upper piezoelectric patch and the host beam, $k_1 = 0$.

2.2. Boundary conditions

The boundary conditions for the smart beam are given as follows:

For the piezoelectric patch, both ends are free, and boundary conditions at each end are

$$T_i = 0; \quad Q_i = 0; \quad M_i = 0; \quad i = 1,3 \tag{8}$$

The relevant boundary conditions of the host beam should also be applied.

2.3. Continuity conditions

At the interface of the debonding area and non-debonding area, to guarantee the continuity of the structure components, the displacements as well as the related internal forces at the debonding interface should be continuous. Therefore, the following continuity conditions are imposed:

$$u_i^p = u_i^d, \quad w_i^p = w_i^d, \quad w_{i,x}^p = w_{i,x}^d, \quad T_i^p = T_i^d, \quad Q_i^p = Q_i^d, \quad M_i^p = M_i^d; \quad i = 1,2,3 \tag{9}$$

where the superscript p and d stand for the displacement in non-debonding and debonding area at the interface line respectively.

3. Sensor equation

When the piezoelectric patch is used as the sensor, there is no external (electric field) voltage applied on it. The charge accumulated on the patch due to the direct piezoelectric effect can be evaluated by

$$q(t) = \frac{b}{2}\int_0^l (D_3|_{z=z_{su}} + D_3|_{z=z_{sl}})\,\mathrm{d}x \tag{10}$$

where D_3 is the electric displacement in thickness direction. The electric charge accumulated on the electrodes of the sensor layer can be obtained by

$$q(t) = \int_{L_n} be_{313}u_{3,x}\,\mathrm{d}x - \int_{L_n} be_{313}r_3w_{3,xx}\,\mathrm{d}x + \int_{L_d} be_{313}u_{3,x}\,\mathrm{d}x - \int_{L_d} be_{313}r_3w_{3,xx}\,\mathrm{d}x \tag{11}$$

where L_n and L_d represent the non-debonding and debonding areas respectively, e_{313} is the piezoelectric stress constant of the sensor layer, and r_3 is the z-coordinate value of the mid-plane of the sensor layer from its own neutral plane.

Differentiating the charge with respect to time, the current output of the sensor can be obtained as

$$I(t) = \int_{L_n} be_{313}u_{3,xt}\,\mathrm{d}x - \int_{L_n} be_{313}r_3w_{3,xxt}\,\mathrm{d}x + \int_{L_d} be_{313}u_{3,xt}\,\mathrm{d}x - \int_{L_d} be_{313}r_3w_{3,xxt}\,\mathrm{d}x \tag{12}$$

The boundary conditions and the continuity conditions are similar as the actuator case in the above section except that the voltage should be zero.

4. Control scheme

4.1. Collocated control

In this case, we use one piezoelectric pair, one of them is used as the actuator and the other is used as sensor. To perform the vibration control of the smart beam, the control laws should be designed to determine the control voltage applied on the piezoelectric actuators. The direct feedback control for the collocated sensor and actuator is widely used and the control voltage is simply designed as

$$V(t) = -g_1q(t) - g_2I(t) \tag{13}$$

where g_1 and g_2 are control gains.

Although the sensor and actuator are bonded onto the upper and lower surfaces of host beam respectively, they are not strictly collocated. In this case, the stability for the higher modes of the closed-loop system cannot be guaranteed when the longitudinal vibration of the smart beam without natural damping is

considered (Yang and Huang, 1998). In practice, the components related to high frequencies should be ruled out by a filter.

4.2. Non-collocated control

In this case, we use two piezoelectric patch pairs, one as the actuator pair and the other as the sensor pair. Using the sensor and actuator pairs, the effect of the longitudinal vibration can be greatly suppressed so that the closed loop system may become more robust.

The charge output of the piezoelectric sensor pair can be obtained by

$$q_{\text{pair}}(t) = q_{\text{u}}(t) - q_{\text{l}}(t) \tag{14}$$

where $q_{\text{u}}(t)$ and $q_{\text{l}}(t)$ are the charge output of the upper and lower sensor patch of the sensor pair respectively which can be obtained from Eq. (11). In Eq. (14), there is no components related to the longitudinal vibration in the output of the sensor pair since the charge generated by the longitudinal vibration is cancelled each other.

To control the transverse vibration of the composite beam, the control voltage of the actuator pair can be designed by the following positive position feedback (PPF) method.

$$\xi_{,tt}(t) + 2\zeta_{\text{c}}\omega_{\text{c}}\xi_{,t}(t) + \omega_{\text{c}}^2\xi(t) = \omega_{\text{c}}^2 q_{\text{pair}}(t) \tag{15}$$

where ζ_{c} and ω_{c} are the damping ratio and natural frequency of the PPF compensator. The control voltage is designed as

$$V(t) = g_p\xi(t) \tag{16}$$

where g_p is the control gain. To control the first mode of the composite beam, the frequency ω_{c} of the compensator should be equal to the first modal frequency of the beam. The advantage of PPF control scheme is that it is not necessary to get the current output of the piezoelectric sensor.

5. Method of solution

The entire beam with piezoelectric patches attached includes several segments, and the governing equations may have different forms in each segment. For the segment including the host beam and two piezoelectric layers without external mechanical load, taking Fourier transformation in Eqs. (1a)–(6b) with respect to time, choosing

$$\mathbf{Y_i} = (\bar{u}_i, \bar{T}_i, \bar{w}_i, \bar{w}_{i,x}, \bar{Q}_i, \bar{M}_i)^{\text{T}}; \quad i = 1, 2, 3 \tag{17}$$

as the state vector (Tong and Steven, 1999), the governing equations can be written as the following state equation

$$\mathbf{Y}_{p,x} = \mathbf{A}_p\mathbf{Y}_p + \mathbf{B}_p\bar{V} \tag{18}$$

where $\mathbf{Y}_p = (\mathbf{Y}_1^{\text{T}}, \mathbf{Y}_2^{\text{T}}, \mathbf{Y}_3^{\text{T}})^{\text{T}}$ is the state vector, $\mathbf{A}_p \in C^{18\times 18}$ is a state matrix, and $\mathbf{B}_p \in C^{18}$ is a vector.

In Eq. (17), the over bar represents the Fourier transformation, for example,

$$\bar{w}_1(x,\omega) = \int_{-\infty}^{\infty} w_1(x,t)\mathrm{e}^{-\mathrm{i}\omega t}\,\mathrm{d}t \tag{19}$$

For the segment of the naked host beam without mechanical load, a similar state equation can be obtained as

$$\mathbf{Y}_{2,x} = \mathbf{A}_h \mathbf{Y}_2 \tag{20}$$

where $\mathbf{A}_h \in C^{6\times 6}$ is a state matrix of the host beam.

The governing equations of different segments of the beam have been transformed into a set of simultaneous ordinary differential equations with parameter ω. After taking Fourier transformation of the their boundary conditions, the governing equations together with their corresponding boundary conditions form a boundary value problem of ordinary differential equations. In this problem, different segment of the composite beam has different governing equations, and even in the segment with piezoelectric patches, the state equation for the debonding area is different from those for the non-debonding areas. Therefore, the multiple shooting method (Stoer and Bulirsch, 1980) is generalized to solve this problem. In this method, the whole beam span is divided into many subintervals and in each subinterval the simple shooting method is used. The solution can be obtained by adjusting the initial values simultaneously in all subintervals until the boundary conditions and the continuity conditions at the points dividing the subintervals are satisfied. Once the solution in each dividing point is solved, the solution over each subinterval can be obtained by solving ordinary differential equations with the values at its starting point as the initial conditions. In the computation, all the interface points are selected as the points dividing the subintervals.

6. Results and discussion

6.1. Validation of the present model

Before discussing the effects of the debonding of the piezoelectric path on vibration control of the beam, a comparison is given between the result obtained by present model and the available experimental and finite element results presented by Seeley and Chattopadhyay (1998, 1999). The host beam is made of a $[0°/90°]_{3s}$ composite material, and its average thickness of the beam is 1.94 mm. The beam is clamped at its left end and its effective length is 30 cm. Two 10.3 cm long and 0.0762 mm thick piezoelectric patches are bonded on the upper and lower surfaces of the composite beam and their left ends are 3.4 cm away from the clamped end. The mass density of the beam and the piezoelectric patch are 1507 and 5000 kg/m^3. The Young's modulus of the piezoelectric patches is 6.9 GPa. The equivalent bending stiffness and extension stiffness for the composite beam with unit width are calculated as: $\bar{D}_2 = 45.5196$ Nm^2, $\bar{A}_2 = 1.19795 \times 10^{10}$ N. In our calculation, the thickness of the adhesive layer is taken as 0.1 mm and its physical properties are given in Table 1.

When the debonding length is taken as 0 (perfect bonding), 1.8, 3.6 and 5.4 cm, the first two modal frequencies of the beam obtained by the present model are listed in Table 2. In Table 2, the results obtained by experiment and finite element method (Seeley and Chattopadhyay, 1998, 1999) based on a refined HOT are also given. Table 2 shows that the first two modal frequencies of the beam with debonded piezoelectric

Table 1
Physical properties and dimensions of the beam with actuator/sensor

Item	Host beam (aluminum)	Piezosensor/actuator	Adhesive layer
Mass density (kg/m^3)	7800	7600	1600
Young's modulus (GPa)	210	63	2.4
Poisson's ratio			0.34
Piezo-constant d_{31} (m/V)	–	370×10^{-12}	–
Thickness (mm)	2	0.4	0.15
Length (mm)	300	50	
Width (mm)	20	20	20

Table 2
Comparison of the natural frequencies (Hz) of the beam with debonded piezoelectric patches

Debonding length (cm)	Current model		Experiment (Seeley and Chattopadhyay, 1998)		HOT (Seeley and Chattopadhyay, 1998)	
	Mode 1	Mode 2	Mode 1	Mode 2	Mode 1	Mode 2
0	25.50	116.36	25.1	120.6	25.4	116.3
1.8	25.19	116.26	24.5	118.7	24.6	115.3
3.6	24.96	118.93	24.6	119.4	24.2	113.2
5.4	24.80	116.58	24.5	120.3	23.8	116.3

patch are in agreement with the experiment and HOT results. The slight difference is due to the fact that, in the present model (1) a thin adhesive layer (0.1 mm) with a lower Young's modulus is considered; (2) the equivalent bending and extensional stiffness of the composite host beam are used; (3) the small accelerometer (0.4 g) on the free end of the host beam used in the experiment is not modeled. The comparison clearly validates the present model and solution scheme.

To validate the control result for the perfectly bonded case, we compare the control results obtained by the present model and an equivalent model. Using the classical laminate beam theory, a host beam fully covered with a piezoelectric actuator and sensor layers can be treated as a single equivalent beam. The exact frequency response of such an equivalent model for a cantilever beam is derived and given in Appendix A. When the dimensions are taken as: $h_2 = 1.2$ mm, $h_1 = h_3 = 0.5$ mm, $L = 16$ cm, $g_2 = 1000$ and the physical parameters are taken from Table 1, the frequency response at the free end of the beam to an initial impulse of 0.1 N s acting at the free end can be obtained using Eq. (A.7), and the frequency spectrum of the charge output sensed by the sensor can also be calculated from Eq. (A.10). The most important information is the location and height of each peak in the spectrum, which indicates the frequency and contribution of the related vibration mode to the response. Table 3 presents the frequencies and peak values related to the first three modes in the frequency spectra of the tip deflection and the sensor output for the equivalent beam model. To make the comparison, when the thickness of the adhesive layer are taken as 0.05, 0.1 and 0.15 mm, the results obtained using the present model are also listed in Table 3. It can be seen from Table 3 that the first three modal frequencies obtained using both models are very close and the differences between them are less than 3%. Although the peak values (heights of resonance peaks) in the frequency spectrum are very sensitive to the change of model, the first modes derived from the two models are still in good agreement when the adhesive layer is very thin. For instance, the maximum deviations between the first two peak values in the spectra of the sensor output and the tip deflection are 5% and 8.7% respectively when the thickness of the adhesive layer is 0.05 mm. The differences between the third peak values in the spectra

Table 3
Comparison of the control results between present model and an equivalent model

	Peak 1 (mode 1)			Peak 2 (mode 2)			Peak 3 (mode 3)		
	Frequency (Hz)	Charge output	Tip defection	Frequency (Hz)	Charge output	Tip defection	Frequency (Hz)	Charge output	Tip defection
Equivalent model	44.22	1.122e−5	3.497e−3	277.70	5.148e−7	4.639e−5	779.30	1.119e−7	6.209e−6
Present model $h_v = 0.05$ mm	43.58 (1.4%)	1.178e−5 (5.0%)	3.800e−3 (8.7%)	273.40 (1.5%)	5.006e−7 (2.8%)	4.328e−5 (6.7%)	763.70 (2.0%)	1.265e−7 (13.1%)	7.751e−6 (24.8%)
Present model $h_v = 0.1$ mm	43.40 (1.9%)	1.199e−5 (6.9%)	3.919e−3 (12.1%)	271.90 (2.1%)	4.966e−7 (3.5%)	4.230e−5 (8.8%)	759.60 (2.5%)	1.314e−7 (17.4%)	8.308e−6 (33.8%)
Present model $h_v = 0.15$ mm	43.20 (2.3%)	1.216e−5 (8.4%)	4.016e−3 (14.8%)	270.70 (2.5%)	4.938e−7 (4.1%)	4.162e−5 (10.3%)	756.30 (3.0%)	1.351e−7 (20.8%)	8.751e−6 (40.9%)

calculated from the two models become remarkable for the cases with thicker adhesive layers. This inconsistence of the control results related to higher modes is due to the fact that the adhesive layers and the longitudinal vibration are not taken into account in the equivalent model. The coupling of the longitudinal and transverse vibration can also affect the active control of the higher modes (Yang and Huang, 1998).

6.2. A numerical example

In this section, an illustrative example is presented to show the effects of partial debonding of the piezoelectric actuator/sensor patches from the host beam on its closed-loop vibration control. Consider a cantilever beam with a pair of piezoelectric wafers being bonded on its upper and lower surfaces and acting as an actuator and a sensor respectively. The host beam is clamped at one end and free at the other, and is subject to an initial transverse impulse loading of 0.1 N s at the free end. Both sensor and actuator patches are made of the same piezoelectric material (PZT-5A) and have the same dimensions. The adhesive layers for bonding the sensor and actuator have the same properties and dimensions as listed in Table 1. Natural damping is not considered in this example.

First of all, we examine the control effect of the collocated control on the beam with a perfectly bonded actuator and sensor pair, which located 2 cm away (location 1) and 6 cm away (location 2) from the clamped end of the beam respectively, as shown in Fig. 3.

When the control gains in Eq. (13) are chosen as $g_1 = 0$, $g_2 = 100{,}000$, the frequency spectrum of the charge output $\bar{q}^p(\omega)$ and the frequency spectrum of the tip deflection $\bar{w}_2^p(L,\omega)$ for the controlled beam with a perfectly bonded actuator/sensor pair are calculated. The amplitude–frequency curves of the normalized frequency spectra, $q_p^*(\omega) = \bar{q}^p(\omega)/\bar{q}^p(0)$ and $w_{2p}^* = \bar{w}_2^p(L,\omega)/\bar{w}_2^p(L,0)$, are shown in Figs. 4 and 5. Figs. 4 and 5 show that the first four modes of the beam are controlled effectively by using the collocated control scheme. When the actuator/sensor pair is bonded at location 1, the first four peeks in the spectrum are located at 20.00, 117.64, 321.25 and 664.39 HZ respectively, and when the actuator/sensor pair is at location 2, the four frequencies are 19.35, 113.87, 329.22 and 658.70 Hz respectively. The control results of the beam with perfectly bonded sensor and actuator patches will be used as a baseline for evaluating the effects of the sensor/actuator debonding on closed-loop vibration control of the beam.

Secondly, we investigate the effects of the actuator debonding on the closed-loop vibration control from two aspects, namely, the effect on the structure of the whole frequency response spectra of the closed-loop system, and the effect on the control efficiency for each controlled modes (i.e. peak values).

When the debonding of 20%, 40% and 80% the actuator length occur at the left end of the actuator patch, the frequency spectra of the sensor output $\bar{q}^d(\omega)$ and the tip displacement $\bar{w}_2^d$ of the closed-loop vibration

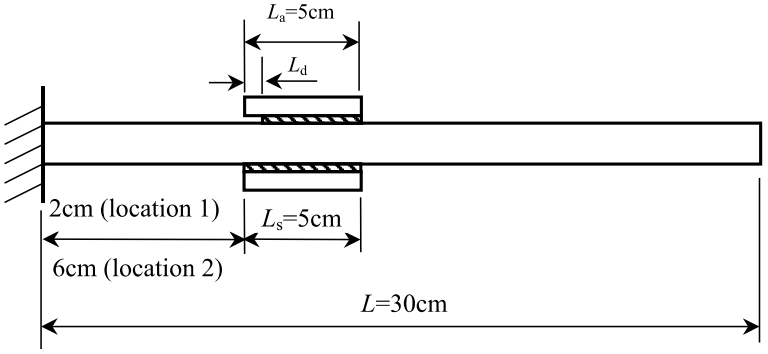

Fig. 3. The cantilever beam with piezoelectric actuator/sensor pairs.

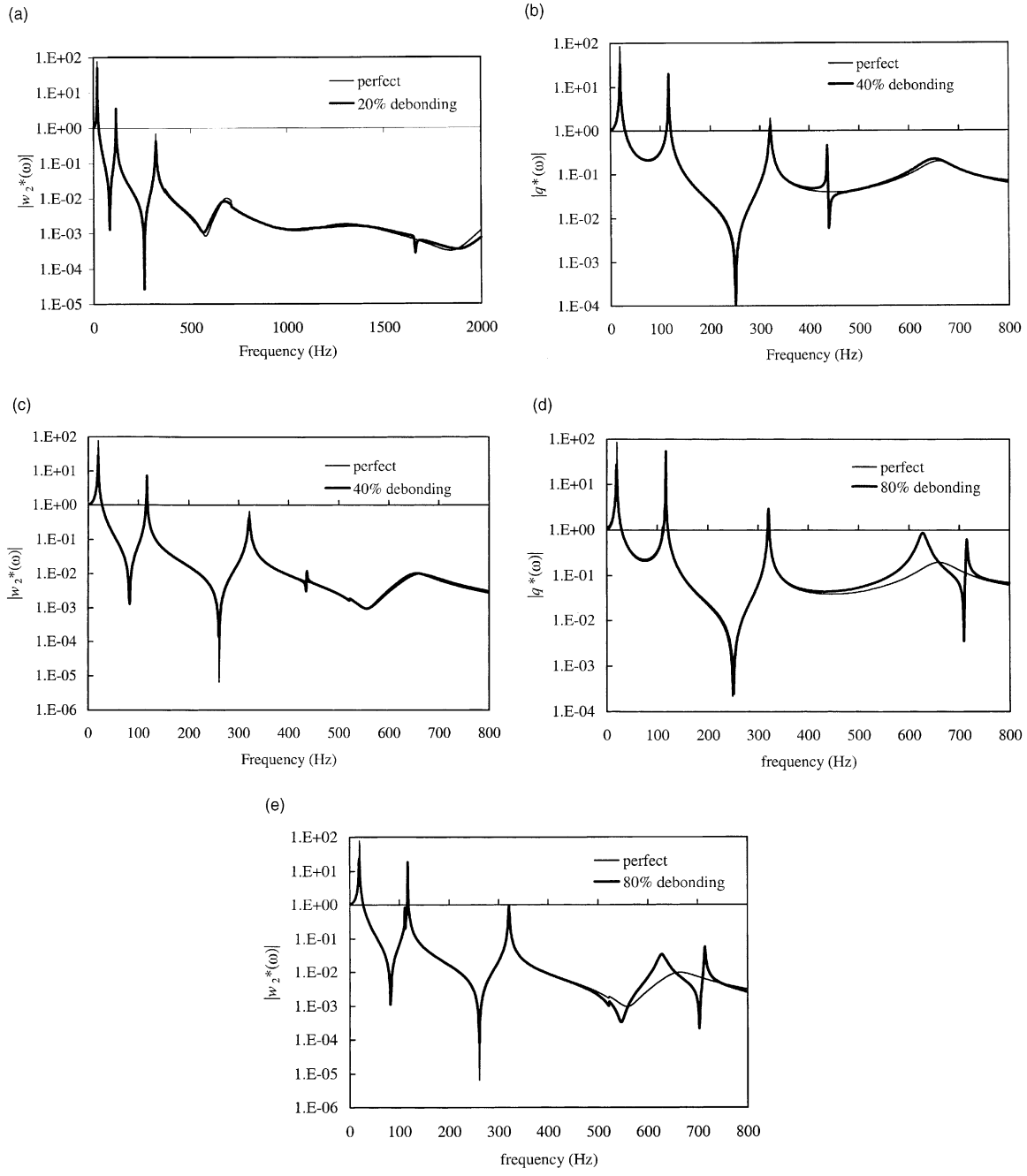

Fig. 4. Frequency spectra of the sensor output and the tip displacement when the actuator/sensor is located at location 1. (a) Tip displacement for 20% debonding, (b) sensor output for 40% debonding, (c) tip displacement for 40% debonding, (d) sensor output for 80% debonding and (e) tip displacement for 80% debonding.

control system in response to an initial impulse are obtained using a frequency increment of 1 Hz. The amplitude–frequency curves of these non-dimensionalized spectra, $q_{\mathrm{d}}^{*}(\omega) = \bar{q}^{d}(\omega)/\bar{q}^{d}(0)$ and $w_{2\mathrm{d}}^{*} =$

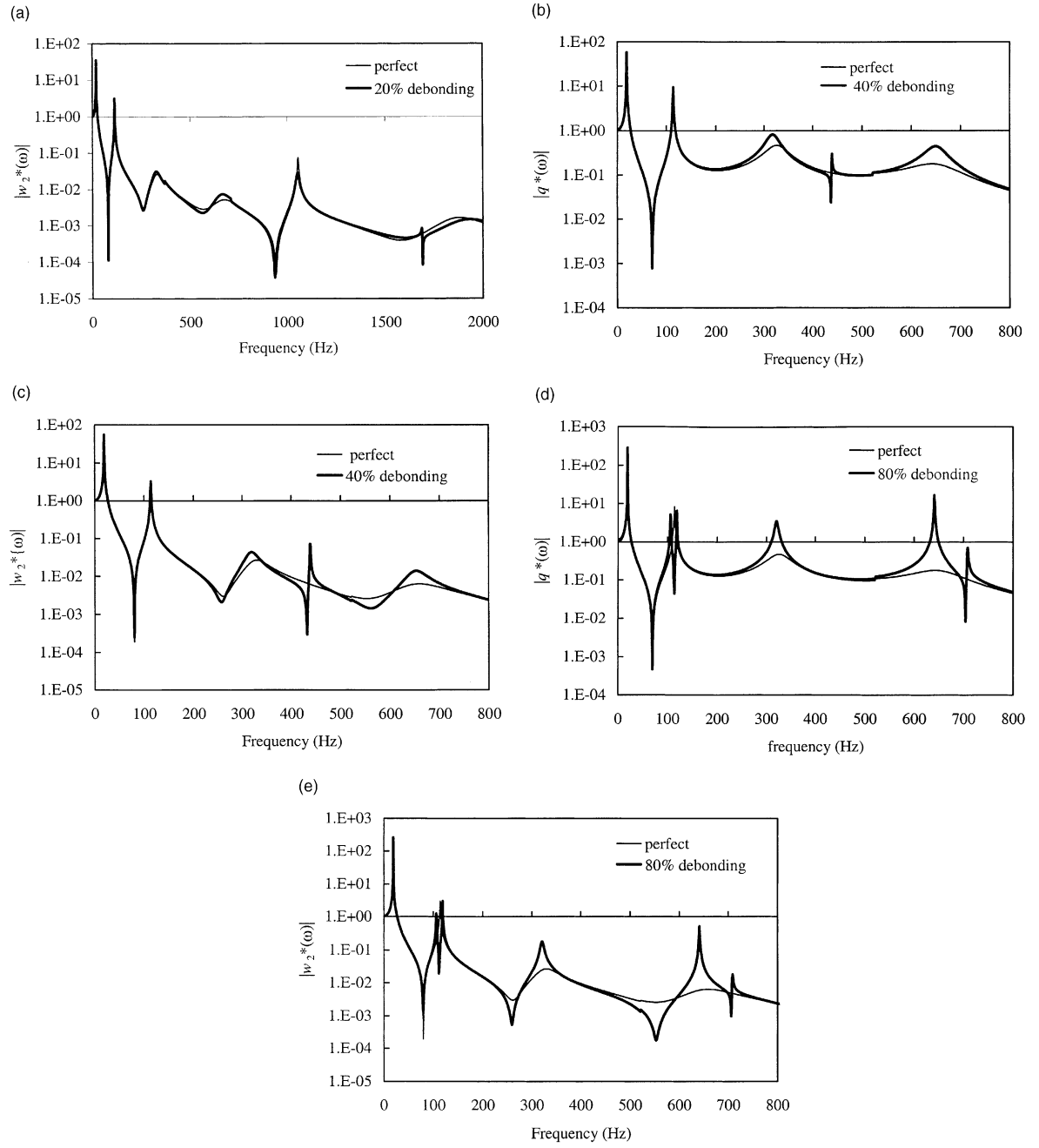

Fig. 5. Frequency spectra of the sensor output and the tip displacement when the actuator/sensor is located at location 2. (a) Tip displacement for 20% debonding, (b) sensor output for 40% debonding, (c) tip displacement for 40% debonding, (d) sensor output for 80% debonding and (e) tip displacement for 80% debonding.

$\bar{w}_2^d(L,\omega)/\bar{w}_2^d(L,0)$, for the case in which the actuator/sensor locates at location 1 are shown in Fig. 4, while those for the case that the actuator/sensor locates at location 2 are presented in Fig. 5. It can be seen

from Figs. 4 and 5 that one or two additional peaks appear in the frequency spectra due to debonding of the actuator patch. It is clear that these additional peaks result from the vibration of the debonded part of the actuator because the debonded part of the actuator can be excited by the dynamic mechanical loading and/or the actuating voltage on the actuator. The debonded part of the actuator behaves like a small cantilever beam whose length equals to the debonding length. For example, when a 1 cm (20%) debonding locates at the left end of the actuator patch, the first natural frequency of the small debonded part of the actuator obtained using the classical beam theory is 1824 Hz, which is larger than the actual one (about 1670 Hz) given in Fig. 4a or 5a due probably to its small debonding length. As the debonding length increases, these two frequencies become closer. For instance, the additional peak due to a 2 cm (40%) edge debonding of the actuator patch appears at 439 Hz, which is slightly smaller than the predicted frequency of the small debonded part of the actuator obtained by the classical beam theory (456.05 Hz), as shown in Fig. 4c or 5c. As depicted in Figs. 4e and 5e, when the debonding length is 4 cm (80% of the actuator), the first frequency for the small beam is 114.03 Hz, which is very close to the actual one (111.12 Hz). This is an interesting feature for the composite beam with debonded actuator, and which may be used to detect the existence of debonding and even estimate the debonding length of the piezoelectric patches. In addition, it should be noted by comparing Figs. 4 and 5 that the vibration of the debonded part of the actuator located at location 1 is larger than that at location 2. This may be because for the first modal the displacement amplitude at location 2 is larger than that at location 1. Figs. 4 and 5 also indicate that unlike the tip displacement, the sensor output is always sensitive to the vibration of the debonded part of the actuator, which may be helpful for debonding detection. As shown in Figs. 4 and 5, when the debonding between the piezoelectric patches and the host beam, the spectrum structure may becomes different due to the appearance of additional peaks. In addition, both location and peak value of each peak corresponding to a vibration mode in the frequency spectrum of the sensor output or the tip defection will change in different degree.

Next, we investigate in details the effects of debonding of actuator patch on vibration control of each mode by examine the changes of its peak values in the frequency spectrum relative to that of the perfectly bonded actuator case. Denote the ith peak value (contribution of the ith mode) in the spectrum of the tip deflection (sensor output) for the perfectly bonding case by $p^p_{wi}(p^p_{si})$, and that with debonded piezoelectric patches by $p^d_{wi}(p^d_{si})$. The relative peak difference of the ith peak in the spectrum of the tip deflection (sensor output) is defined by $R_{wi} = (|p^d_{wi}| - |p^p_{wi}|)/|p^p_{wi}|(R_{si} = (|p^d_{si}| - |p^p_{si}|)/|p^p_{si}|)$. The effect of the debonding of the piezoelectric patches on each mode of the closed loop control can be evaluated from its related peak difference in the frequency spectra. Fig. 6 presents the relative peak differences for both sensor output and tip deflection versus the normalized debonding length L_d/L_a of the actuator patch when the debonding occurs at the left end of the actuator, which also includes the results for the two cases in which the actuator/sensor locates at location 1 and 2. When the actuator locates at location 2, the relative peak differences related to the first four modes become significant when the edge debonding occurs. For example, when a 20% edge debonding of the actuator occurs, the first four relative peak differences in the spectrum of the tip deflection reach 32%, 5%, 20% and 48% respectively, which means that a 20% edge debonding results in a 32%, 5%, 20% and 48% increase of the peak values in the spectrum of the tip deflection related to the first four vibration modes respectively; whereas a 40% debonding of the actuator leads to a 87%, 23%, 63% and 120% increase of the peak values corresponding to the first four modes respectively. Even a 10% edge debonding of the actuator leads to an increase in peak values for the first four modes by 14%, 1%, 9% and 20% respectively. For the case that the sensor and actuator pair is placed at location 1, the debonding also increases the peak values corresponding to the first two modes. In this case, a 20% debonding of the actuator increases the peak values related to the first and second modes by 33% and 76% respectively. As the debonding length increases, the relative peak difference corresponding to the second mode enlarges dramatically because of the special location of the actuator (see Fig. 6b). It is also worth noting that a 10% debonding of the actuator can cause a 31% increase of the second peak value in the spectrum of the tip

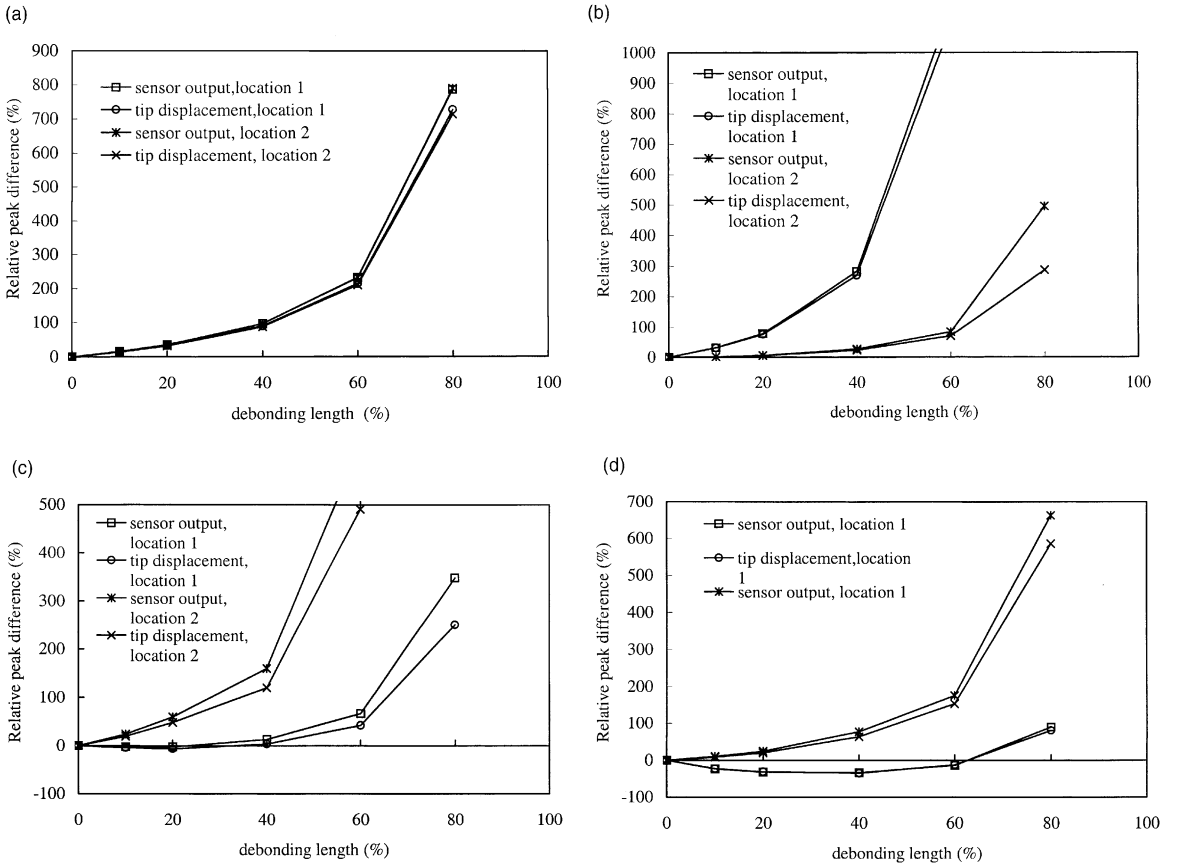

Fig. 6. Relative peak differences R_{wi} and R_{si} $(i = 1,4)$ of peak values in frequency spectrum versus non-dimensionalized debonding length of actuator patch L_d/L_a (edge debonding). (a) Mode 1, (b) mode 2, (c) mode 3 and (d) mode 4.

deflection. However, the effect of the actuator debonding on the control of the third and fourth modes is different. Instead of increasing the peaks related to the third and fourth modes, the 20% edge debonding causes a decrease of 31% and 2% respectively. This phenomenon can be explained from the viewpoint of the modal influence coefficient (Sun et al., 2001). It is known that the actuating ability to a specific mode depends on its modal influence coefficient, which is related to the difference between the strains at the actuator's ends for a beam. In this case, in addition to the decrease of the actuating ability caused by a debonding, the debonding makes the effective part of the actuator coincide to the node of the second modal strain. As a result, the modal influence coefficient for the second mode becomes very small and thus leads to an extreme increase of the second mode. In general, debonding of the actuator worsens the control effect, however, this may not be true for some modes when the actuator is located at some special locations, as shown in Fig. 6c. In this case, the debonding increases the modal influence coefficient for mode 3 and therefore the control of this mode is improved. This phenomenon occurs because the actuator happens to cover one node of the third strain mode. Another possible reason for this phenomenon is that the third and fourth modes are totally destabilized by the debonding. In conclusion, even a small debonding of the actuator can significantly worsen the closed loop control of the first four modes when the actuator/sensor pair does not cover any nodes of their corresponding strain modes.

When the natural frequencies of the debonded part of the actuator approach to one of the frequencies of the composite beam, resonance occurs. Hence, the effect of such a debonding on the closed loop control is particularly concerned. For the case that the sensor/actuator pair locates at location 1, when the debonding length is 4 cm, the first natural frequency of the debonded actuator part is close to the second modal frequency of the beam. In this case, the effects of such a debonding on control of the third mode is presented in Fig. 7. In Fig. 7a, λ stands for the ratio of the first modal frequency of the debonded actuator part and the second modal frequency of the beam. Fig. 7a indicates that the resonance debonding length is near 79% of the total length of the actuator. It can be seen from Fig. 7b that the vibration amplitude of the debonded actuator gets very larger when its first modal frequency approaches the second frequency of the beam. However, the amplitude of the second mode of the beam becomes smaller due to the resonance, as shown in Fig. 7c. This is possibly because the energy of the second vibration mode flows into the debonded actuator and the debonded actuator functions as a dynamic vibration absorber.

When the debonding occurs at the left end of the sensor patch, its effect on closed loop control is also investigated for the case that the sensor/actuator pair is located at location 2. Fig. 8a depicts the relative

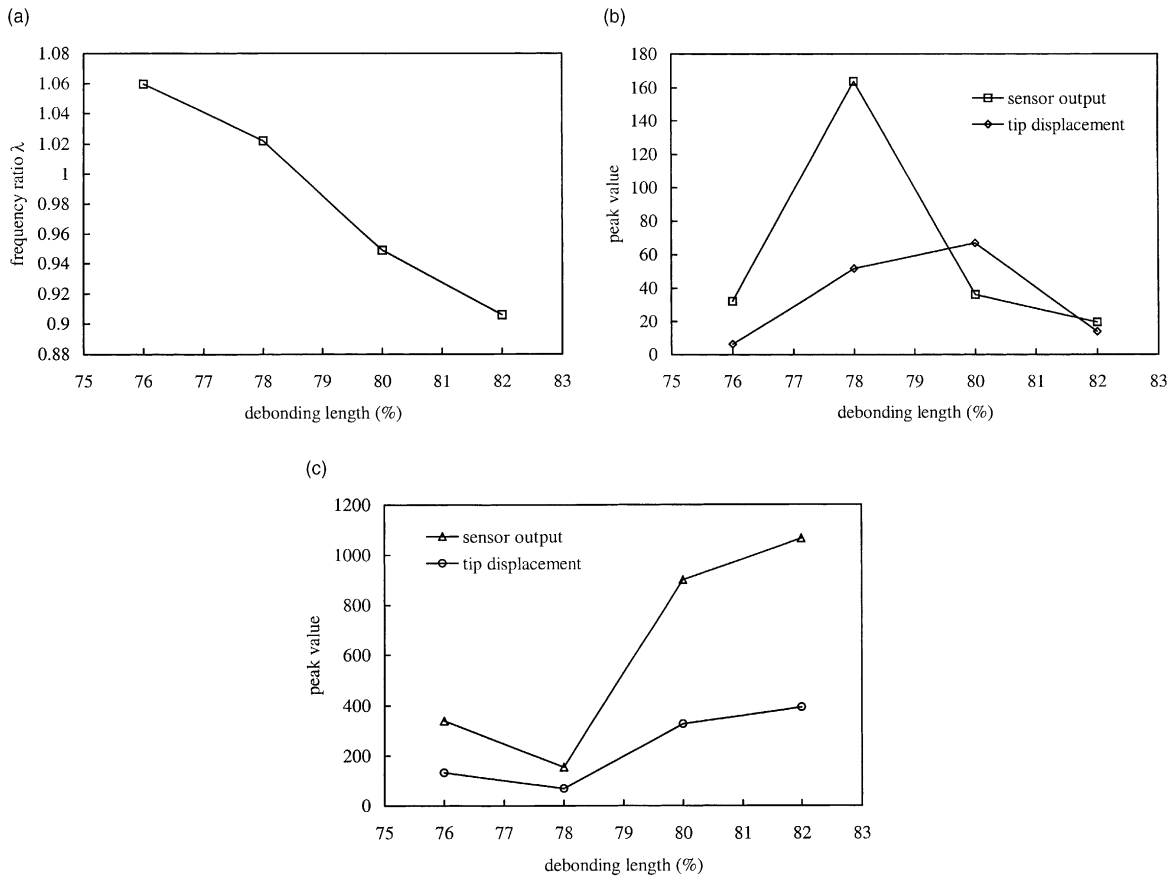

Fig. 7. Resonance effects of actuator debonding on control of mode 2 of the beam. (a) Ratio of the first frequency of the debonded actuator and the second modal frequency of the beam, (b) peak values related to the first mode of the debonded actuator via debonding length and (c) peak values related to the second mode of the beam via debonding length.

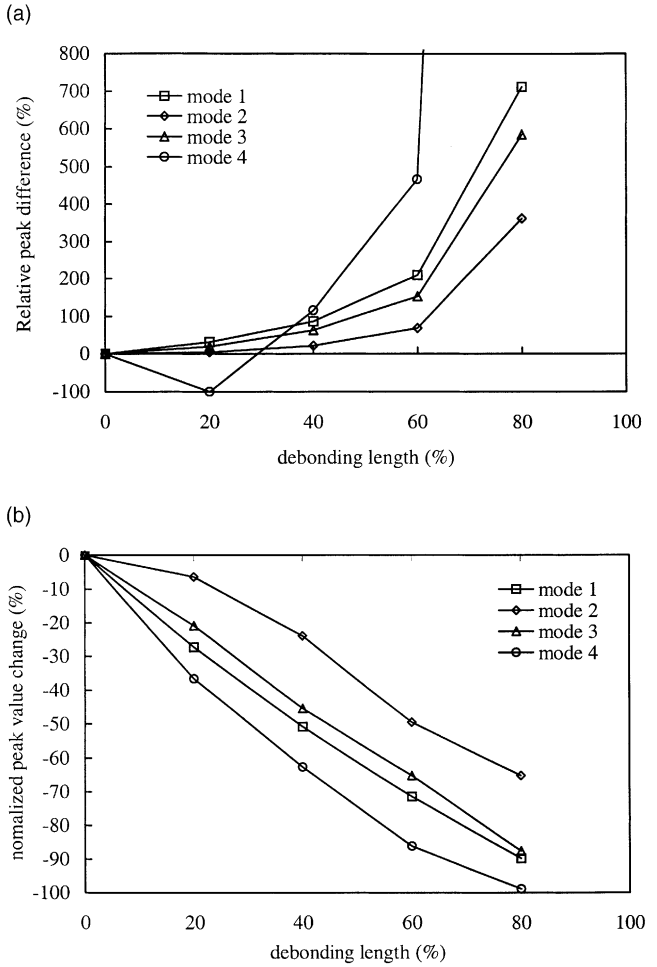

Fig. 8. Effects of sensor debonding on control of the first modes (actuator/sensor at location 1). (a) Tip displacement and (b) peak values decrease in the sensor output relative to perfect case.

peak differences of the first four peak values in the frequency spectrum of the tip transverse displacement with different debonding length of the sensor. It is shown that the control of the first three modes is greatly worsened, which is similar to the actuator debonding case. For example, a 20% edge debonding of the sensor lead to 32%, 5%, 20% increase of the peak values corresponding to the first three modes in the spectrum of the charge output, and when a 40% debonding of the sensor patch occurs, the relative peak differences for the first four peaks in the spectrum of the charge output reach as high as 87%, 22%, 63% and 116% respectively. Fig. 8b presents changes of the four peak values in the frequency spectrum of the sensor output from the debonded sensor, which is normalized by those of perfectly bonded sensor. For example, a 20% debonding of the sensor patch decrease the first four peak values in the spectrum of the charge output by 27%, 6%, 21% and 37% respectively. Fig. 8b reflects that the sensed signals are nearly linearly weakened with the increase of the debonding length. However, such a linear decrease of the sensor output result in a exponential increase of the vibration amplitude of the controlled beam because the vibration amplitude is very sensitive to active damping provided by the closed loop control.

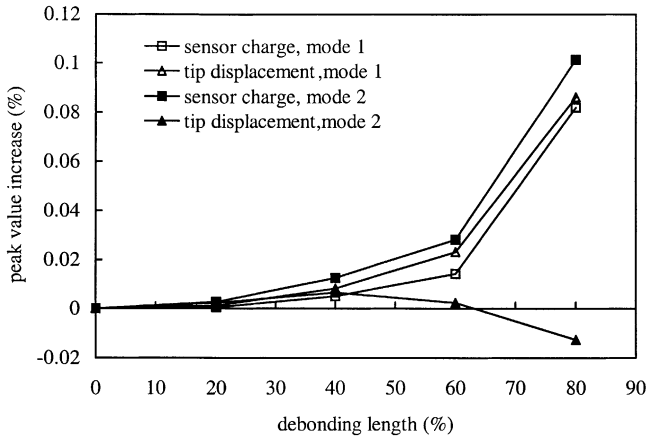

Fig. 9. Relative peak differences R_{wi} and R_{si} $(i = 1, 2)$ of peak values in frequency spectrum versus non-dimensionalized debonding length of actuator patch L_d/L_a (mid debonding).

When the debonding locates in the middle of the actuator patch (in location 2), the changes of the peak values related to the first two modes with different debonding length are drawn in Fig. 9. It is clear that the closed-loop vibration control of the beam is only slightly affected by the debonding in the middle of the actuator patch. The increases of amplitude of the two controlled modes are less than 0.11% even when a 80% debonding occurs in the middle of the actuator patch.

Finally, we compare the tolerant capabilities of the control system with single actuator patch and with actuator pair to the debonding of the actuator. To this end, a 5 cm long actuator pair is bonded 2 cm away from the clamped end of the beam to its left end, and the sensor pair with the same length as the actuator is located 8 cm away from the clamped end. The non-collocated control law in Eqs. (15) and (16) is employed to design the control voltage from the charge output of the sensor pair. The damping ratio and the frequency of the compensator are chosen as: $\zeta_c = 0.5$, $\omega_c = 131.32$ (the first natural frequency of the composite beam). The control gain g_p in Eq. (16) is taken as 10^6. For the case the only one actuator of the

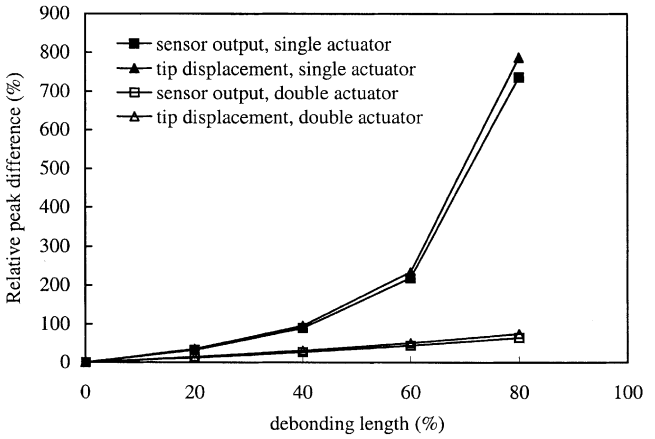

Fig. 10. Relative peak differences R_{w1} and R_{s1} of peak values in frequency spectrum versus non-dimensionalized debonding length of actuator patch L_d/L_a using non-collocated control.

actuator pair is used, when debonding occurs at the end of active actuator patch, its effect on the control of the first mode is depicted in Fig. 10. Again, similar to the collocated control case, the control of the first mode is significantly worsened by the actuator. For example, when a 20% debonding locates at the left end of the actuator patch, a 35% relative peak increase of the first peak value in the spectrum of the tip deflection can be observed. However, if both actuator patches are used, the effect of the debonding of the actuator on the control of the first mode is much weaker, as shown in Fig. 10. In this case, a 20% debonding in one of the two actuator patches lead to a 15% increase of the first peak value in the spectrum of the tip deflection. It can be concluded that a single actuator is much more sensitive to the debonding than an actuator pair.

7. Conclusions

In this paper, an analytical model is presented for closed-loop vibration control of a smart beam with partially debonded piezoelectric sensor/actuator patches based on the classical beam theory. In this model, both flexural and longitudinal displacements of the host beam and the piezoelectric layers are considered, and the adhesive layer is modeled. Using the displacements and their corresponding internal forces as the state variables, a numerical approach based on the multiple shooting method is employed to solve the equations, and the both displacement and force continuities are satisfied in the interface between the debonded and non-debonded areas. Form present simulation results, the effects of the debonding of the actuator/sensor on closed loop control of the beam are identified via the following observations:

1. The debonding of the actuator/sensor affects the structure of the frequency spectrum of the closed loop system. Not only the vibration of the composite beam, but also the vibration of the debonded part of the actuator/sensor is included in the spectrum of the output of the sensor during the control process.
2. A debonding located at the end of the actuator or sensor can significantly worsen the control of the first several modes of the beam if the actuator or sensor does not cover any nodal points of the vibration modes.
3. When one frequency of the debonded portion of the actuator/sensor is close to one modal frequency of the composite beam, the close-loop control of such mode of the beam is particularly affected in such a way that the output of the sensor may not pick up the dynamic information for this mode accurately.
4. The debonding locates at the middle of the actuator/sensor has very little effects on the active control and the frequencies of the closed-loop vibration system if the first frequency of the debonded portion of an actuator/sensor is remarkably different from those of the controlled modes.
5. A single actuator is much more sensitive to debonding than an actuator pair in the closed-loop vibration control of the beam.

Acknowledgements

The authors are grateful to the support of the Australian Research Council via a Large Grant (grant no. A10009074).

Appendix A

Consider a cantilever beam fully covered with piezoelectric actuator and sensor layers on its upper and lower surfaces respectively. Assume that the piezoelectric layers are perfectly bonded on the host beam and the effects of the bonding layers between the piezoelectric layers and the host beam on the composite beam

are negligible. In this case, the composite beam is usually treated as an equivalent single beam. When the longitudinal vibration of the beam is not considered, the equation of motion of the equivalent beam has the form (Lee and Moon, 1990)

$$\rho_{\mathrm{eq}} w_{,tt} + D_{\mathrm{eq}} w_{,xxxx} = -be_{31a} r_a V_{,xx} + f(x,t) \tag{A.1}$$

where $w(x,t)$ is the transverse displacement of the composite beam, ρ_{eq} and D_{eq} are the equivalent mass density per unit length and the equivalent bending stiffness of the composite beam respectively, r_a is the z-coordinate of the mid-plane of the actuator layer measured from the neutral plane of the composite beam, $V(x,t)$ is the control voltage applied on the actuator, $f(x,t)$ is the applied transverse excitation.

The charge and current output from the piezoelectric sensor can be written as

$$q(t) = -be_{313} r_s \int_0^L w_{,xx}\,\mathrm{d}x = -be_{313} r_s [w_{,x}(L,t) - w_{,x}(0,t)] \tag{A.2}$$

$$I(t) = -be_{313} r_s \int_0^L w_{,xxt}\,\mathrm{d}x = -be_{313} r_s [w_{,xt}(L,t) - w_{,xt}(0,t)] \tag{A.3}$$

where r_s is the z-coordinate of the mid-plane of the actuator layer measured from the neutral plane of the composite beam, L is the length of the beam.

When a uniform control voltage $V(t)$ designed by the control law

$$V(t) = -g_2 I(t) \tag{A.4}$$

the closed-loop control of the cantilever beam becomes a boundary control described by

$$\begin{aligned} &\rho_{\mathrm{eq}} w_{,tt} + D_{\mathrm{eq}} w_{,xxxx} = f(x,t) \\ &w(0,t) = 0; \qquad w_{,x}(0,t) = 0 \\ &w_{,xx}(L,t) = -\frac{be_{311} r_a V(t)}{D_{\mathrm{eq}}}; \qquad w_{,xxx}(L,t) = \frac{F(t)}{D_{\mathrm{eq}}} \end{aligned} \tag{A.5}$$

where $F(t)$ is a point force acting at the free end of the beam. Substituting Eqs. (A.3) and (A.4) into Eq. (A.5), and taking Fourier transformation with respect to t in Eq. (A.5), the frequency response of the controlled composite beam to an initial impulse of I_p (i.e. $F(t) = I_p \delta(t)$) applied at its free end can be solved from

$$\begin{aligned} &-\rho_{\mathrm{eq}} \omega^2 \bar{w} + D_{\mathrm{eq}} \bar{w}_{,xxxx} = 0 \\ &\bar{w}(0) = 0; \qquad \bar{w}_{,x}(0) = 0 \\ &\bar{w}_{,xx}(L) = \alpha \bar{w}_{,x}; \qquad \bar{w}_{,xxx}(L) = \frac{I_p}{D_{\mathrm{eq}}} \end{aligned} \tag{A.6}$$

where $\bar{w}(x,\omega)$ is the Fourier transformation of the displacement $w(x,t)$, and $\alpha = gi\omega b^2 e_{311} e_{313} r_a r_s / D_{\mathrm{eq}}$.

The solution of Eq. (A.6) can be derived as

$$\bar{w}(x,\omega) = C_1(\omega)(\cos\beta x - \cosh\beta x) + C_2(\omega)(\sin\beta x - \sinh\beta x) \tag{A.7}$$

where

$$\begin{aligned} &\beta^4 = \rho_{\mathrm{eq}} \omega^2 / D_{\mathrm{eq}} \\ &C_1(\omega) = \tfrac{I_p}{D_{\mathrm{eq}}|A|}[\beta(\sin\beta L + \sinh\beta L) + \alpha(\cos\beta L - \cosh\beta L)] \\ &C_2(\omega) = \tfrac{I_p}{D_{\mathrm{eq}}|A|}[-\beta(\cos\beta L + \cosh\beta L) + \alpha(\sin\beta L + \sinh\beta L)] \end{aligned} \tag{A.8}$$

with

$$A = \begin{bmatrix} -\beta(\cos\beta L + \cosh\beta L) + \alpha(\sin\beta L + \sinh\beta L) & -\beta(\sin\beta L + \sinh\beta L) - \alpha(\cos\beta L - \cosh\beta L) \\ \beta^3(\sin\beta L - \sinh\beta L) & -\beta^3(\cos\beta L + \cosh\beta L) \end{bmatrix} \tag{A.9}$$

when $\alpha = 0$, $|A| = 0$ gives the well-known characteristic equation of the cantilever beam.

After taking Fourier transformation in Eq. (A.2), the charge output of the sensor for the cantilever beam becomes

$$\bar{q}(\omega) = -be_{313}r_s\bar{w}_{,x}(L,\omega) \tag{A.10}$$

which measures the rotation angle of the beam at its free end.

References

Baz, A., Poh, S., 1988. Performance of an active control system with piezoelectric actuators. Journal of Sound and Vibration 126, 327–343.

Chandrashekhara, K., Agarwal, A.N., 1993. Active vibration control of laminated composite plates using piezoelectric devices: A finite element approach. Journal of Intelligent Material Systems and Structures 4, 496–508.

Chee, C., Tong, L., Steven, G.P., 1998. A review on the modeling of piezoelectric sensors and actuators incorporated in intelligent structures. Journal of Intelligent Material Systems and Structures 9, 3–19.

Crawley, E.F., 1994. Intelligent structures for aerospace: A technology overview and assessment. AIAA Journal 32, 1689–1699.

Gu, Y., Clark, R.L., Fuller, C.R., 1994. Experiments on active control of plate vibration using piezoelectric actuators and polyvinylidene fluoride (PVDF) modal sensors. Journal of Vibration and Acoustics 116, 303–308.

Lee, C.-K., Moon, F.C., 1990. Modal sensors and actuators. Journal of applied mechanics 57, 434–441.

Im, S., Atluri, S.N., 1989. Effect of a piezo-actuator on a finitely deformed beam subject to general loading. AIAA Journal 27, 1801–1807.

Seeley, C.E., Chattopadhyay, A., 1998. Experimental investigation of composite beams with piezoelectric actuation and debonding. Smart Materials and Structures 7, 502–511.

Seeley, C.E., Chattopadhyay, A., 1999. Modeling of adaptive composites including debonding. International Journal of Solids and Structures 36, 1823–1843.

Shi, G., Atluri, S.N., 1990. Active control of nonlinear dynamic response of space-frames using piezo-electric actuators. Computer and Structures 34, 549–564.

Stoer, J., Bulirsch, R., 1980. Introduction to numerical analysis. Springer, New York, pp. 483–519.

Sun, D.C., Wang, D.J., Xu, Z.L., 1999. Distributed piezoelectric element method for vibration control of smart plates. AIAA Journal 39, 1459–1463.

Sun, D.C., Tong, L., 2001a. Modal control of smart shells by optimized discretely distributed piezoelectric transducers. International Journal of Solids and Structures 38, 3281–3299.

Sun, D.C., Tong, L., 2001b. Sensor/actuator equations for curved piezoelectric fibers and vibration control of composite beams using fiber modal actuators/sensors. Journal of Sound and Vibration 241, 297–314.

Sun, D.C., Tong, L., Wang, D.J., 2001. Vibration control of plates using discretely distributed piezoelectric quasi-modal actuator/sensors. AIAA Journal 39, 1766–1772.

Tong, L., Steven, G.P., 1999. Analysis and design of structural bonded joints. Kluwer, Dordrecht.

Tzou, H-S., Anderson, G.L., 1992. Intelligent Structural Systems. Kluwer, Dordrecht.

Wang, X.D., Meguid, S.A., 2000. On the electroelastic behaviour of a thin piezoelectric actuator attached to an infinite host structures. International Journal of Solids and Structures 37, 3231–3251.

Yang, S.Y., Huang, W.H., 1998. Is a collocated piezoelectric sensor/actuator pair feasible for an intelligent beam? Journal of sound and vibration 216, 529–538.